PHYSICAL REVIEW B **93**, 161411(R) (2016)

Theory of third-harmonic generation in graphene: A diagrammatic approach

Habib Rostami[*] and Marco Polini
Istituto Italiano di Tecnologia, Graphene Labs, Via Morego 30, I-16163 Genova, Italy
(Received 3 February 2016; published 25 April 2016)

We present a finite-temperature diagrammatic perturbation theory of third-harmonic generation in doped graphene. We carry out calculations of the third-order conductivity in the scalar potential gauge, highlighting a subtle cancellation between a Fermi surface contribution, which contains only power laws, and power-law contributions of interband nature. Only logarithms survive in the final result. We conclude by presenting quantitative results for the upconversion efficiency at zero and finite temperature. Our approach can be easily generalized to other materials and to include many-body effects.

DOI: 10.1103/PhysRevB.93.161411

Introduction. The nonlinear optical properties of graphene [1], the most studied two-dimensional (2D) material, are beginning to attract considerable interest. Using four-wave mixing, Hendry *et al.* [2] demonstrated experimentally that the third-order optical susceptibility of graphene is remarkably large ($\approx 1.4 \times 10^{-15}$ m^2/V^2) and only weakly dependent on wavelength in the near-infrared frequency range. Third-harmonic generation (THG) from mechanically exfoliated graphene sheets has been measured by Kumar *et al.* [3] who extracted a value of the third-order susceptibility on the order of 10^{-16} m^2/V^2 for an incident photon energy $\hbar\omega = 0.72$ eV. Finally, Hong *et al.* [4] reported strong THG in graphene grown by chemical vapor deposition, in a situation in which the incident photon energy $\hbar\omega = 1.57$ eV is in three-photon resonance with the exciton-shifted van Hove singularity.

A large body of theoretical work on THG in graphene has appeared in the recent literature [5–9]. In Ref. [6], a power-law singularity (a second-order pole) at $\hbar\omega = 2E_{\rm F}$ was found in the third-order conductivity, for both clean and disordered systems. Moreover, a logarithmic resonance at $\hbar\omega = E_{\rm F}$ was missed. In Ref. [7], the clean-system result (see below) for the third-order conductivity agrees with the corresponding result of Refs. [8,9]. According to Refs. [7–9], the clean-limit third-order conductivity displays a total of three logarithmic contributions at $\hbar\omega = 2E_{\rm F}/3$, $E_{\rm F}$, and $2E_{\rm F}$, with the main THG peak occurring at $\hbar\omega = 2E_{\rm F}/3$.

In this Rapid Communication we present a finite-temperature diagrammatic perturbation theory of THG in graphene (see Fig. 1). Our approach has the advantage of being transparent and easily extendable to 2D materials with a more complex band structure such as graphene derivatives (e.g., bilayer graphene), transition-metal dichalcogenides, and few-layer black phosphorus. Being based on Green's functions, our approach can also be combined with *ab initio* methods for materials that are poorly described by low-energy continuum models. Also, it can be generalized [10–12] to take into account electron-electron interactions (plasmons, excitons, etc.).

We carry out microscopic calculations of THG in a noninteracting 2D system of massless Dirac fermions (MDFs) [13] in the *scalar potential gauge* (SPG). In this gauge, light-matter interactions are described by utilizing an external scalar potential, which couples to the electronic density operator. As explained in Ref. [14], this gauge is free of the pathologies that one encounters when optical properties of 2D MDFs are calculated by employing the *vector potential gauge* and the MDF current operator, which lacks a diamagnetic contribution [15]. Furthermore, in the vector potential gauge, light-matter interactions are described through the minimal coupling $\boldsymbol{p} \to \boldsymbol{p} + e\boldsymbol{A}(t)/c$ in the continuum-model Hamiltonian. The vector potential is time dependent but uniform, implying that in this gauge the momentum $\hbar\boldsymbol{q}$ of incident photons is set to zero from the very beginning. Although this choice tremendously simplifies analytical calculations, it is known to miss intraband (i.e., Fermi surface) contributions.

Here, we report an *a priori* unexpected cancellation between the Fermi surface contribution to the third-order conductivity, which contains only power laws, and power-law contributions of interband nature. Only logarithms survive

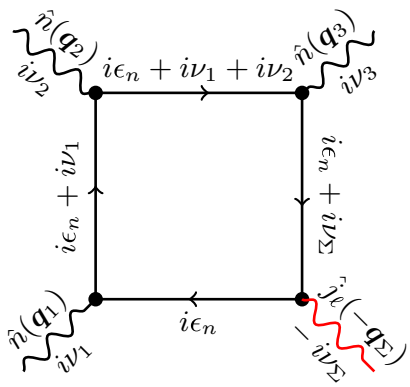

FIG. 1. Example of a four-leg diagram for the third-order response tensor $\Pi^{(3)}_{\ell}(-\nu_\Sigma;\nu_1,\nu_2,\nu_3|-\boldsymbol{q}_\Sigma;\boldsymbol{q}_1,\boldsymbol{q}_2,\boldsymbol{q}_3)$ in the SPG. Solid lines indicate noninteracting Matsubara Green's functions. Black wavy lines indicate scalar potentials (incoming photons) carrying a finite wave vector $\boldsymbol{q}_i$ and energy ν_i with $i = 1\ldots3$. The red wavy line denotes a scalar potential (outgoing photon) carrying a wave vector $\boldsymbol{q}_\Sigma$ and energy ν_Σ. Conservation of momentum and energy require $\boldsymbol{q}_\Sigma = \sum_i \boldsymbol{q}_i$ and $\nu_\Sigma = \sum_i \nu_i$, respectively. Black dots indicate external vertices. Here, ν_i (ϵ_n) denotes a bosonic (fermionic) Matsubara energy.

[*]Habib.Rostami@iit.it

in the final result. This anomalous cancellation occurs for all values of the microscopic parameters and is not tied to the linear dispersion of MDFs in single-layer graphene. For example, we have checked (not shown here) that it also occurs for massive chiral fermions in bilayer graphene [1]. Also, we have checked (not shown here) that it occurs (i) in the presence of terms that break particle-hole symmetry (e.g., next-nearest-neighbor hopping in the tight-binding model) and (ii) for anisotropic 2D MDFs (e.g., uniaxially strained graphene). We believe that this cancellation stems from the gapless nature of the dispersion relation, as power-law terms are present in the final result for THG in gapped graphene [5]. (However, the calculations of Ref. [5] are in the vector potential gauge.) Finally, we note that the failure to fulfill this cancellation may be at the origin of the rich variety of results that have appeared in the recent literature [5–9].

Diagrammatic perturbation theory of THG. We consider the single-channel Hamiltonian of a 2D system of noninteracting MDFs [13], $\hat{\mathcal{H}}_0 = v_{\rm F}\int d^2\boldsymbol{r}\,\hat{\psi}^\dagger(\boldsymbol{r})(\boldsymbol{\sigma}\cdot\boldsymbol{p})\hat{\psi}(\boldsymbol{r})$, where $v_{\rm F}\sim 10^6$ m/s is the graphene Fermi velocity, $\hat{\psi}(\boldsymbol{r}) = [\hat{\psi}_{\rm A}(\boldsymbol{r}),\hat{\psi}_{\rm B}(\boldsymbol{r})]^{\rm T}$, $\boldsymbol{\sigma} = (\sigma_x,\sigma_y)$ is a 2D vector of Pauli matrices, and $\boldsymbol{p} = -i\hbar\nabla_{\boldsymbol{r}}$. We calculate THG by using perturbation theory in an external *homogeneous* time-dependent electric field $\boldsymbol{E}(t)$. The latter induces a current, which can be formally expanded in powers of the electric field, $J_\ell = \sum_n J_\ell^{(n)}$, where $n = 1,2,3,\ldots$ denotes the order in perturbation theory and $\ell = x,y$ is a Cartesian index. Due to spatial inversion symmetry, the second-order ($n = 2$) response to a uniform electric field is identically zero [16,17]. The third-order conductivity tensor $\boldsymbol{\sigma}^{(3)}$ is defined as follows:

$$J_\ell^{(3)}(\omega_\Sigma) = \sum_{\alpha_1\cdots\alpha_3}\sigma^{(3)}_{\ell\alpha_1\alpha_2\alpha_3}(-\omega_\Sigma;\omega_1,\omega_2,\omega_3)\Pi_{i=1}^3 E_{\alpha_i}(\omega_i), \quad (1)$$

where $\alpha_1\cdots\alpha_n = x,y$ are Cartesian indices, E_{α_i} denotes the α_ith Cartesian component of $\boldsymbol{E}$, and $\omega_\Sigma = \sum_i\omega_i$. The first-order conductivity tensor $\boldsymbol{\sigma}^{(1)}(-\omega;\omega)$, which controls linear optics [18,19], is defined in Ref. [20].

Coupling of the electronic degrees of freedom described by $\hat{\mathcal{H}}_0$ to the electric field of incident light can be described in different electromagnetic gauges [21]. In the SPG, light-matter interactions are described by adding a scalar potential to the Hamiltonian, i.e., $\hat{\mathcal{H}}_V = \hat{\mathcal{H}}_0 + \int d^2\boldsymbol{r}\,V(\boldsymbol{r},t)\hat{n}(\boldsymbol{r})$. Here, $\hat{n}(\boldsymbol{r})$ is the density operator and $V(\boldsymbol{r},t) = -e\Phi(\boldsymbol{r},t)$, where $\Phi(\boldsymbol{r},t) = \mathcal{S}^{-1}[\varphi(\boldsymbol{q},\omega)e^{i(\boldsymbol{q}\cdot\boldsymbol{r}-\omega t)}e^{\eta t/\hbar} + \text{c.c.}]/2$ is the electric potential and $\mathcal{S}$ the 2D electron system area. The quantity $\eta = 0^+$ is the usual positive infinitesimal [21], which is needed to make sure that the field vanishes in the remote past ($t\to-\infty$). The Fourier components of the electric field are given by $\boldsymbol{E}(\boldsymbol{q},\omega) = -i\boldsymbol{q}\varphi(\boldsymbol{q},\omega)$. In order to have a finite electric field, the photon wave vector $\boldsymbol{q}$ must be kept finite in this gauge. The uniform $|\boldsymbol{q}|\to 0$ limit can be taken only at the end of the calculation. In the SPG we are therefore able to take into account *both* intra- and interband contributions to optical response tensors.

In the SPG, the third-order conductivity tensor $\boldsymbol{\sigma}^{(3)}$ can be obtained from

$$\sigma^{(3)}_{\ell\alpha_1\alpha_2\alpha_3} = \frac{(-i)^3(-e)^3}{\mathcal{N}!}\frac{\partial^3\Pi_\ell^{(3)}}{\partial q_{1,\alpha_1}\partial q_{2,\alpha_2}\partial q_{3,\alpha_3}}\bigg|_{\{\boldsymbol{q}_i\to\boldsymbol{0}\}}, \quad (2)$$

where $\mathcal{N}!$ originates from the Taylor expansion in powers of $\boldsymbol{q}_i$. The rank-1 tensor $\Pi_\ell^{(3)}(-\nu_\Sigma;\nu_1,\nu_2,\nu_3|-\boldsymbol{q}_\Sigma;\boldsymbol{q}_1,\boldsymbol{q}_2,\boldsymbol{q}_3)$ is a sum of Feynman diagrams such as the one in Fig. 1:

$$\Pi_\ell^{(3)} = \frac{ev_{\rm F}N_{\rm f}}{3!}\int\frac{d^2\boldsymbol{k}}{(2\pi)^2}\sum_{\lambda_1\cdots\lambda_4=\pm}\sum_{\mathcal{P}}F_{\lambda_1\cdots\lambda_4}(\boldsymbol{k},\boldsymbol{q}_1,\boldsymbol{q}_2,\boldsymbol{q}_3)I_{\lambda_1\cdots\lambda_4}(\boldsymbol{k},\boldsymbol{q}_1,\boldsymbol{q}_2,\boldsymbol{q}_3,\nu_1,\nu_2,\nu_3), \quad (3)$$

where

$$\begin{aligned}F_{\lambda_1\cdots\lambda_4} = {}& \langle\lambda_1,\boldsymbol{k}|\hat{n}(\boldsymbol{q}_1)|\lambda_2,\boldsymbol{k}+\boldsymbol{q}_1\rangle\langle\lambda_2,\boldsymbol{k}+\boldsymbol{q}_1|\hat{n}(\boldsymbol{q}_2)|\lambda_3,\boldsymbol{k}+\boldsymbol{q}_1+\boldsymbol{q}_2\rangle\langle\lambda_3,\boldsymbol{k}+\boldsymbol{q}_1+\boldsymbol{q}_2|\hat{n}(\boldsymbol{q}_3)|\lambda_4,\boldsymbol{k}+\boldsymbol{q}_\Sigma\rangle\\ &\times\langle\lambda_4,\boldsymbol{k}+\boldsymbol{q}_\Sigma|\frac{\hat{\boldsymbol{j}}_\ell(-\boldsymbol{q}_\Sigma)}{-ev_{\rm F}}|\lambda_1,\boldsymbol{k}\rangle\end{aligned} \quad (4)$$

is a dimensionless form factor due to the four external vertices, while

$$I_{\lambda_1\cdots\lambda_4} = \frac{1}{\beta}\sum_{i\epsilon_n}[G(i\epsilon_n,\varepsilon_{\lambda_1,\boldsymbol{k}})G(i\epsilon_n+i\nu_1,\varepsilon_{\lambda_2,\boldsymbol{k}+\boldsymbol{q}_1})G(i\epsilon_n+i\nu_1+i\nu_2,\varepsilon_{\lambda_3,\boldsymbol{k}+\boldsymbol{q}_1+\boldsymbol{q}_2})G(i\epsilon_n+i\nu_\Sigma,\varepsilon_{\lambda_4,\boldsymbol{k}+\boldsymbol{q}_\Sigma})] \quad (5)$$

is due to the presence of four Green's functions in Fig. 1. In Eq. (3), $N_{\rm f} = 4$ is the number of fermion flavors in graphene [13] and $\sum_{\mathcal{P}}$ denotes a sum over the $3! = 6$ permutations of the energy and wave vector variables $\{\nu_i,\boldsymbol{q}_i\}$ of the three incoming photons [16,17] in Fig. 1. In Eq. (4), $\hat{n}(\boldsymbol{q})$ and $\hat{\boldsymbol{j}}(\boldsymbol{q})$ are the Fourier transforms of the density $\hat{n}(\boldsymbol{r})$ and paramagnetic current $\hat{\boldsymbol{j}}(\boldsymbol{r})$ operators, respectively, where $\hat{\boldsymbol{j}}(\boldsymbol{r}) = -ev_{\rm F}\hat{\psi}^\dagger(\boldsymbol{r})\boldsymbol{\sigma}\hat{\psi}(\boldsymbol{r})$, $-e$ being the electron charge. Since there is no vector potential in the SPG, we do not need to worry about diamagnetic contributions [15] to the paramagnetic current operator $\hat{\boldsymbol{j}}(\boldsymbol{r})$. In Eq. (5), $\beta = 1/(k_{\rm B}T)$, where T is temperature, $\epsilon_n = (2n+1)\pi/\beta$ is a fermionic Matsubara energy, and $G(i\epsilon_n,\varepsilon_{\lambda,\boldsymbol{k}}) = 1/(i\epsilon_n-\varepsilon_{\lambda,\boldsymbol{k}})$ is the bare Green's function in the band representation, with $\varepsilon_{\lambda,\boldsymbol{k}} = \lambda\hbar v_{\rm F}|\boldsymbol{k}|$ for conduction ($\lambda = +$) and valence ($\lambda = -$) band states.

To make progress, we must *first* perform the sum over the fermionic Matsubara energy ϵ_n in Eq. (5). This can actually be done analytically by following standard textbook tricks [21]. Only *after* can one carry out the analytical continuation $i\nu_i\to\hbar\omega_i + i\eta$ to real photon energies $\hbar\omega_i$. The end result of this procedure for the case of harmonic generation [16,17], i.e., $\omega_i = \omega$ and $\boldsymbol{q}_i = \boldsymbol{q}$,

and the $\ell = x$ component of $\Pi^{(3)}_\ell$ is

$$\begin{aligned}\Pi^{(3)}_x(-3\omega;\omega,\omega,\omega|-3\boldsymbol{q};\boldsymbol{q},\boldsymbol{q},\boldsymbol{q})&\\ = N_{\rm f} e v_{\rm F}\int\frac{d^2\boldsymbol{k}}{(2\pi)^2}\sum_{\lambda_1\cdots\lambda_4=\pm}\frac{F_{\lambda_1\cdots\lambda_4}(\boldsymbol{k},\boldsymbol{q},\boldsymbol{q},\boldsymbol{q})}{3(\hbar\omega+i\eta)+\varepsilon_{\lambda_1,\boldsymbol{k}}-\varepsilon_{\lambda_4,\boldsymbol{k}+3\boldsymbol{q}}}&\\ \times\Bigg\{\Bigg[\frac{1}{2(\hbar\omega+i\eta)+\varepsilon_{\lambda_1,\boldsymbol{k}}-\varepsilon_{\lambda_3,\boldsymbol{k}+2\boldsymbol{q}}}\Bigg\{\frac{n_{\rm F}(\varepsilon_{\lambda_1,\boldsymbol{k}})-n_{\rm F}(\varepsilon_{\lambda_2,\boldsymbol{k}+\boldsymbol{q}})}{\hbar\omega+\varepsilon_{\lambda_1,\boldsymbol{k}}-\varepsilon_{\lambda_2,\boldsymbol{k}+\boldsymbol{q}}+i\eta}-\frac{n_{\rm F}(\varepsilon_{\lambda_2,\boldsymbol{k}+\boldsymbol{q}})-n_{\rm F}(\varepsilon_{\lambda_3,\boldsymbol{k}+2\boldsymbol{q}})}{\hbar\omega+\varepsilon_{\lambda_2,\boldsymbol{k}+\boldsymbol{q}}-\varepsilon_{\lambda_3,\boldsymbol{k}+2\boldsymbol{q}}+i\eta}\Bigg\}\Bigg]&\\ +\Bigg[\frac{1}{2(\hbar\omega+i\eta)+\varepsilon_{\lambda_2,\boldsymbol{k}+\boldsymbol{q}}-\varepsilon_{\lambda_4,\boldsymbol{k}+3\boldsymbol{q}}}\Bigg\{\frac{n_{\rm F}(\varepsilon_{\lambda_3,\boldsymbol{k}+2\boldsymbol{q}})-n_{\rm F}(\varepsilon_{\lambda_4,\boldsymbol{k}+3\boldsymbol{q}})}{\hbar\omega+\varepsilon_{\lambda_3,\boldsymbol{k}+2\boldsymbol{q}}-\varepsilon_{\lambda_4,\boldsymbol{k}+3\boldsymbol{q}}+i\eta}-\frac{n_{\rm F}(\varepsilon_{\lambda_2,\boldsymbol{k}+\boldsymbol{q}})-n_{\rm F}(\varepsilon_{\lambda_3,\boldsymbol{k}+2\boldsymbol{q}})}{\hbar\omega+\varepsilon_{\lambda_2,\boldsymbol{k}+\boldsymbol{q}}-\varepsilon_{\lambda_3,\boldsymbol{k}+2\boldsymbol{q}}+i\eta}\Bigg\}\Bigg]\Bigg\}.\end{aligned}\tag{6}$$

In Eq. (6),

$$F_{\lambda_1\cdots\lambda_4}(\boldsymbol{k},\boldsymbol{q},\boldsymbol{q},\boldsymbol{q})=\frac{1+\lambda_1\lambda_2 e^{i[\phi(\boldsymbol{k}+\boldsymbol{q})-\phi(\boldsymbol{k})]}}{2}\frac{1+\lambda_2\lambda_3 e^{i[\phi(\boldsymbol{k}+2\boldsymbol{q})-\phi(\boldsymbol{k}+\boldsymbol{q})]}}{2}\frac{1+\lambda_3\lambda_4 e^{i[\phi(\boldsymbol{k}+3\boldsymbol{q})-\phi(\boldsymbol{k}+2\boldsymbol{q})]}}{2}\frac{\lambda_1 e^{i\phi(\boldsymbol{k})}+\lambda_4 e^{-i\phi(\boldsymbol{k}+3\boldsymbol{q})}}{2}\tag{7}$$

is the form factor in the SPG, $\phi(\boldsymbol{k})$ being the polar angle of $\boldsymbol{k}$, while $n_{\rm F}(E)=\{\exp[\beta(E-\mu)]+1\}^{-1}$ is the usual Fermi-Dirac distribution function, μ being the finite-T chemical potential. THG in graphene is therefore the result of a complicated interplay between three different families of electron-hole transitions: intraband transitions (i.e., $\lambda_1=\lambda_2=\lambda_3=\lambda_4$), interband transitions (i.e., $\lambda_1=-\lambda_2=\lambda_3=-\lambda_4$), and "hybrid" transitions (e.g., $\lambda_1=\lambda_2=\lambda_3=-\lambda_4$). The latter ones are of course absent in the first-order tensor $\boldsymbol{\sigma}^{(1)}$. In total, there are 12 contributions of a "hybrid" nature, resulting from both intra- and interband processes along the fermion loop in Fig. 1.

We are now in the position to take the uniform $|\boldsymbol{q}|\to 0$ limit by expanding Eqs. (6) and (7) in powers of $\boldsymbol{q}$. We hasten to emphasize that for the case $\boldsymbol{q}_1=\boldsymbol{q}_2=\boldsymbol{q}_3=\boldsymbol{q}$ the expansion of the form factor $F_{\lambda_1\cdots\lambda_4}(\boldsymbol{k},\boldsymbol{q},\boldsymbol{q},\boldsymbol{q})$ up to third order in $\boldsymbol{q}$ cannot be obtained by simply expanding each factor in Eq. (7) up to linear order in $\boldsymbol{q}$. However, when all $\boldsymbol{q}_i$'s differ from each other, as in the general case of Eq. (3), such linearization is legitimate [7]. After lengthy but straightforward calculations, we obtain the desired result for THG generation in graphene:

$$\sigma^{(3)}_{xxxx}=\widetilde{\sigma}_{xxxx;1}+\widetilde{\sigma}_{xxxx;2}+\sigma_{xxxx;\rm FS}.\tag{8}$$

The last term on the right-hand side of Eq. (8), $\sigma_{xxxx;\rm FS}$, is a Fermi surface contribution, which is controlled by an integral over energy whose integrand is pinned at the Fermi surface by the first, second, and third derivatives of $n_{\rm F}(E)$:

$$\begin{aligned}\sigma_{xxxx;\rm FS}=i\kappa\int_0^\infty dE\{&[n'_{\rm F}(E)+n'_{\rm F}(-E)]f(E)\\ &+[n''_{\rm F}(E)-n''_{\rm F}(-E)]g(E)\\ &+[n'''_{\rm F}(E)+n'''_{\rm F}(-E)]h(E)\},\end{aligned}\tag{9}$$

where $\kappa=N_{\rm f}e^4\hbar v_{\rm F}^2/(32\pi)$, $n'_{\rm F}(E)$ is shorthand for the derivative $dn_{\rm F}(E)/dE$, and $n'_{\rm F}(-E)$ is a shorthand for $n'_{\rm F}(E)|_{E\to -E}$. (Similar shorthand expressions have been used for the second and third derivatives.) Explicit expressions for the functions $f(E)$, $g(E)$, and $h(E)$ are reported in Ref. [20]. The terms $\widetilde{\sigma}_{xxxx;1}$ and $\widetilde{\sigma}_{xxxx;2}$ are defined by

$$\widetilde{\sigma}_{xxxx;1,2}=i\kappa\int_0^\infty dE[n_{\rm F}(E)-n_{\rm F}(-E)]F_{1,2}(E),\tag{10}$$

where

$$\begin{aligned}F_1(E)=\Bigg\{&\frac{1}{E^2(\hbar\omega_+)^3}+\frac{4}{(\hbar\omega_+)^2}\Bigg[\frac{1}{(\hbar\omega_++2E)^3}\\ &+\frac{1}{(\hbar\omega_+-2E)^3}\Bigg]-\frac{8}{(\hbar\omega_+)^3}\Bigg[\frac{1}{(\hbar\omega_++2E)^2}\\ &+\frac{1}{(\hbar\omega_+-2E)^2}\Bigg]+\frac{2}{(\hbar\omega_+)^3}\Bigg[\frac{1}{(\hbar\omega_++E)^2}\\ &+\frac{1}{(\hbar\omega_+-E)^2}\Bigg]\Bigg\}\end{aligned}\tag{11}$$

and

$$\begin{aligned}F_2(E)=\Bigg\{&-\frac{8}{3(\hbar\omega_+)^4}\Bigg[\frac{1}{\hbar\omega_++E}+\frac{1}{\hbar\omega_+-E}\Bigg]\\ &+\frac{17}{12(\hbar\omega_+)^4}\Bigg[\frac{1}{\hbar\omega_++2E}+\frac{1}{\hbar\omega_+-2E}\Bigg]\\ &+\frac{5}{4(\hbar\omega_+)^4}\Bigg[\frac{1}{\hbar\omega_++2E/3}+\frac{1}{\hbar\omega_+-2E/3}\Bigg]\Bigg\}.\end{aligned}\tag{12}$$

In Eqs. (11) and (12) we have introduced the shorthand $\omega_+\equiv\omega+i\eta/\hbar$. Note that, for large E, $F_1(E)$ decays faster than $1/E$, while $F_2(E)$ decays exactly as $1/E$. As a consequence, $\widetilde{\sigma}_{xxxx;1}$ ($\widetilde{\sigma}_{xxxx;2}$) contains power laws (logarithms). The explicit calculation of $\widetilde{\sigma}_{xxxx;1,2}$ does not require an ultraviolet cutoff, which would break gauge invariance [14,15,22].

Due to the form of the integrand in Eq. (10) and for its similarity with the integrand in the second term in curly brackets in Eq. (S2) of Ref. [20], we will refer to $\widetilde{\sigma}_{xxxx;1}$ and $\widetilde{\sigma}_{xxxx;2}$ as "interband" contributions to the third-order conductivity. Integrating Eq. (9) by parts, it is possible to show [20] that the following equality holds true:

$$\sigma^{\rm FS}_{xxxx}(-3\omega;\omega,\omega,\omega)=-\widetilde{\sigma}_{xxxx;1}(-3\omega;\omega,\omega,\omega).\tag{13}$$

We therefore conclude that $\sigma_{xxxx}(-3\omega;\omega,\omega,\omega)=\widetilde{\sigma}_{xxxx;2}(-3\omega;\omega,\omega,\omega)$. Equation (13) is the most important result of this work and implies the *absence* of power-law terms in the final result for $\sigma_{xxxx}(-3\omega;\omega,\omega,\omega)$. In the $T=0$

limit, we find

$$\sigma^{(3)}_{xxxx}(-3\omega;\omega,\omega,\omega) = \frac{i\kappa}{24(\hbar\omega_+)^4}[17\mathcal{G}_\eta(\hbar\omega,2|E_{\rm F}|) - 64\mathcal{G}_\eta(\hbar\omega,|E_{\rm F}|) + 45\mathcal{G}_\eta(\hbar\omega,2|E_{\rm F}|/3)], \quad (14)$$

where $\mathcal{G}_\eta(\hbar\omega,E) = \ln[(E+\hbar\omega_+)/(E-\hbar\omega_+)]$. The final result for THG can be obtained by taking the limit $\eta \to 0^+$ in Eq. (14), with $\mathcal{G}_{\eta\to 0^+}(\hbar\omega,E) = \ln|(E+\hbar\omega)/(E-\hbar\omega)| + i\pi\Theta(|\hbar\omega|-E)$. Finally, we observe that Eq. (14) is well behaved in the undoped $E_{\rm F}\to 0$ limit, i.e.,

$$\lim_{E_{\rm F}\to 0}\lim_{\eta\to 0^+}\sigma^{(3)}_{xxxx}(-3\omega;\omega,\omega,\omega) = \frac{\pi\kappa}{12(\hbar\omega)^4}. \quad (15)$$

Equation (14) was first derived by Cheng *et al.* [8] by utilizing a density-matrix approach.

Since the third-order conductivity is known analytically at $T=0$, finite-T effects are most conveniently studied by using the Maldague identity [21]. In our case, this yields the following integral representation for the third-order conductivity at $T\neq 0$:

$$\sigma^{(3)}_{xxxx}\big|_{T\neq 0} = \beta\int_{-\infty}^{\infty} dE\,\frac{\sigma^{(3)}_{xxxx}\big|_{\{T=0,E_{\rm F}\to E\}}}{4\cosh^2[\beta(E-\mu)/2]}, \quad (16)$$

where the $T=0$ result $\sigma^{(3)}_{xxxx}|_{\{T=0,E_{\rm F}\to E\}}$ can be obtained from Eq. (14). The chemical potential as a function of T can be found by solving $\beta^2E_{\rm F}^2 = 2|{\rm Li}_2[-\exp(-\beta\mu)] - {\rm Li}_2[-\exp(\beta\mu)]|$, where ${\rm Li}_2[x]$ is the dilogarithm function. In the limit $\eta\to 0^+$, the real part of $\sigma^{(3)}_{xxxx}$ can be written in a closed form for any value of T and $E_{\rm F}$:

$${\rm Re}\big[\sigma^{(3)}_{xxxx}\big] = \frac{\pi\kappa}{24(\hbar\omega)^4}[2+17n_{\rm F}(\hbar\omega/2) - 64n_{\rm F}(\hbar\omega) + 45n_{\rm F}(3\hbar\omega/2)]. \quad (17)$$

We were not able to find a similar analytical expression for ${\rm Im}[\sigma^{(3)}_{xxxx}]$ at arbitrary T. For an undoped system, $\mu=0$ at any T and ${\rm Im}[\sigma^{(3)}_{xxxx}]=0$.

At this stage, one may be tempted to take into account disorder by introducing a phenomenological relaxation time τ through the replacement $\eta\to\hbar/\tau$ or $\omega_+\to\omega+i/\tau$. In general, this procedure yields a "nonconserving" approximation [23] for optical and transport response functions. The case of the ordinary density-density response function is discussed in Refs. [21,24]. In the diagrammatic language, this replacement takes into account disorder-induced self-energy corrections to response functions, while conserving approximations require one to treat on an equal footing the self-energy *and* vertex corrections. This is why in this work we present results for the clean system and postpone the analysis of THG in disordered graphene sheets to future work.

Upconversion efficiency. For the sake of completeness, we finally present our predictions for the efficiency of the THG process in a clean graphene sheet at finite T. Using the relation $\boldsymbol{J}^{(n)}(\omega) = -i\omega_+\boldsymbol{P}^{(n)}(\omega)$ between the Fourier transforms of the induced current and polarization $\boldsymbol{P}^{(n)}(t)$, we find $P^{(3)}_\ell(\omega_\Sigma) = (i/\omega_{\Sigma,+})\sum_{\alpha_1\cdots\alpha_3}\sigma^{(3)}_{\ell\alpha_1\cdots\alpha_3}\prod_{i=1}^3 E_{\alpha_i}(\omega_i)$, where $\omega_{\Sigma,+}\equiv\omega_\Sigma+i\eta/\hbar$. Assuming a monochromatic incident light beam, linearly polarized along the $\hat{\boldsymbol{x}}$ direction, we find the following expression for the THG intensity, $I^{(3)}(3\omega)$, in units of the first-order intensity $I^{(1)}(\omega)$:

$$\frac{I^{(3)}(3\omega)}{I^{(1)}(\omega)} \equiv \left|\frac{P^{(3)}_x(3\omega)}{P^{(1)}_x(\omega)}\right|^2 = \left[\frac{2I_{\rm i}}{3n_{\rm r}\epsilon_0 c}\right]^2\left|\frac{\sigma^{(3)}_{xxxx}}{\sigma^{(1)}_{xx}}\right|^2. \quad (18)$$

Here, $I_{\rm i} = n_{\rm r}\epsilon_0 c|\boldsymbol{E}|^2/2$ is the intensity of incident light where $|\boldsymbol{E}|$ is the time average of the incident electric field, $\epsilon_0\simeq 8.85\times10^{-12}$ C/(V m) is the vacuum permittivity, $c\simeq 3\times10^8$ m/s, and $n_{\rm r}\simeq 1$. The quantity $I^{(3)}(3\omega)/I^{(1)}(\omega)$ is shown in Fig. 2 for an incident power $I_{\rm i}=1$ GW/cm^2. (This is the peak power used in on-going experiments on THG in doped graphene sheets.) According to Eq. (14), there are three logarithmic divergences at photon energies $\hbar\omega = 2E_{\rm F}/3$, $E_{\rm F}$, and $2E_{\rm F}$ in the $T=0$ expression of $\sigma^{(3)}_{xxxx}$ (marked by vertical dashed lines in the figure). The main THG peak occurs at $\hbar\omega = 2E_{\rm F}/3$. Finite-$T$ effects rapidly smooth out these singularities.

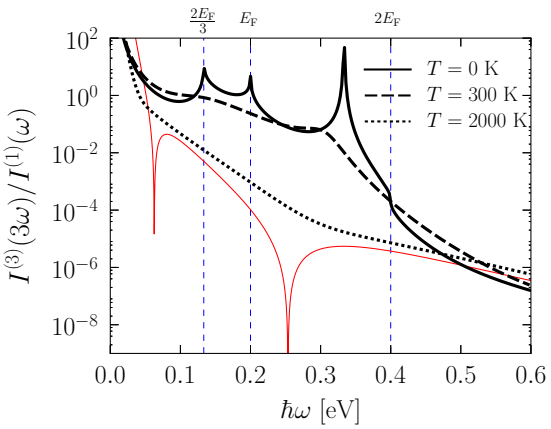

FIG. 2. The ratio $I^{(3)}(3\omega)/I^{(1)}(\omega)$ for a clean graphene sheet—see Eq. (18)—is plotted as a function of the incident photon energy $\hbar\omega$ (in eV), for an incident power $I_{\rm i}=1$ GW/cm^2, and three different values of temperature T. For this plot we have set $E_{\rm F}=200$ meV. The solid red line represents the result for undoped graphene at $T=2000$ K and $\mu=0$. The dashed vertical lines label the three relevant photon frequencies for THG: $\hbar\omega = 2E_{\rm F}/3$, $E_{\rm F}$, and $2E_{\rm F}$. The peak which is *not* marked by a vertical dashed line is due to a zero in the linear-response quantity $I^{(1)}(\omega)$ in Eq. (18) and is unrelated to THG.

The large peak at $\hbar\omega\simeq 1.667E_{\rm F}$ is due to the fact that intra- and interband contributions to the first-order conductivity $\sigma^{(1)}_{xx}$ cancel out [25] at this photon frequency and at $T=0$, yielding $|\sigma^{(1)}_{xx}(-\omega;\omega)|=0$. The undoped result at finite T (solid red line) shows two sharp structures at photon energies $\hbar\omega\simeq 0.362/\beta$ and $\hbar\omega\simeq 1.462/\beta$, which correspond to solutions of the equation $|\sigma^{(3)}_{xxxx}(-3\omega;\omega,\omega,\omega)|=0$ in the undoped case, as it can be readily checked by utilizing Eq. (17). For illustration purposes, in Fig. 2 we show the undoped result at $T=2000$ K (solid red line). In general, we note that graphene is a highly nonlinear material at low frequencies [26].

To compare with available experimental results, we introduce the third-order susceptibility as $\chi^{(3)} = i\sigma^{(3)}/(3\omega\epsilon_0 d)$, where $d\simeq 0.33$ nm is an effective graphene thickness. For example, for $\hbar\omega=0.72$ eV, $E_{\rm F}=0.2$ eV, and $T=300$ K, we obtain $|\chi^{(3)}|\simeq 4.56\times10^{-19}$ m^2/V^2. This value is three

orders of magnitude *smaller* than that measured in Ref. [3]. This discrepancy may stem from a variety of effects that we have not included in our theory, including disorder, many-body effects, and band-structure effects beyond the MDF model.

In summary, we have presented a diagrammatic theory of THG in doped graphene. We have carried out explicit calculations in the scalar potential gauge, discovering an exact cancellation between the Fermi surface contribution to the third-order conductivity and power-law contributions of interband nature. Only logarithms survive in the final result, Eq. (14). We believe that the failure to fulfill this cancellation may be at the origin of the rich variety of results that have appeared in the recent literature. Calculations of THG can also be carried out in the vector potential gauge, but in this case, for the reasons mentioned above, it is safer to use lattice Hamiltonians rather than the MDF model—see, e.g., Ref. [27] for the case of second-harmonic generation in the presence of broken inversion symmetry.

Acknowledgments. We thank G. Cerullo, A. C. Ferrari, S. A. Jafari, and M. I. Katsnelson for many useful discussions. This work was supported by Fondazione Istituto Italiano di Tecnologia and the European Union's Horizon 2020 research and innovation programme under Grant Agreement No. 696656 GrapheneCore1.

[1] A. K. Geim and K. S. Novoselov, Nat. Mater. **6**, 183 (2007).
[2] E. Hendry, P. J. Hale, J. Moger, A. K. Savchenko, and S. A. Mikhailov, Phys. Rev. Lett. **105**, 097401 (2010).
[3] N. Kumar, J. Kumar, C. Gerstenkorn, R. Wang, H.-Y. Chiu, A. L. Smirl, and H. Zhao, Phys. Rev. B **87**, 121406(R) (2013).
[4] S.-Y. Hong, J. I. Dadap, N. Petrone, P.-C. Yeh, J. Hone, and R. M. Osgood, Jr., Phys. Rev. X **3**, 021014 (2013).
[5] S. A. Jafari, J. Phys.: Condens. Matter **24**, 205802 (2012).
[6] S. A. Mikhailov, Phys. Rev. B **90**, 241301(R) (2014); **91**, 039904(E) (2015).
[7] S. A. Mikhailov, Phys. Rev. B **93**, 085403 (2016).
[8] J. L. Cheng, N. Vermeulen, and J. E. Sipe, New J. Phys. **16**, 053014 (2014).
[9] J. L. Cheng, N. Vermeulen, and J. E. Sipe, Phys. Rev. B **91**, 235320 (2015); **93**, 039904(E) (2016).
[10] J. Yu and W. P. Su, Phys. Rev. B **44**, 13315 (1991).
[11] S. A. Jafari, T. Tohyama, and S. Maekawa, J. Phys. Soc. Jpn. **75**, 083706 (2006).
[12] M. I. Katsnelson and A. I. Lichtenstein, J. Phys.: Condens. Matter **22**, 382201 (2010).
[13] V. N. Kotov, B. Uchoa, V. M. Pereira, F. Guinea, and A. H. Castro Neto, Rev. Mod. Phys. **84**, 1067 (2012).
[14] S. H. Abedinpour, G. Vignale, A. Principi, M. Polini, W.-K. Tse, and A. H. MacDonald, Phys. Rev. B **84**, 045429 (2011).
[15] L. Chirolli, M. Polini, V. Giovannetti, and A. H. MacDonald, Phys. Rev. Lett. **109**, 267404 (2012).
[16] L. D. Landau and E. M. Lifshitz, *Course of Theoretical Physics: Electrodynamics of Continuous Media* (Pergamon, New York, 1984).
[17] R. W. Boyd, *Nonlinear Optics* (Academic, London, 2008).
[18] F. Bonaccorso, Z. Sun, T. Hasan, and A. C. Ferrari, Nat. Photonics **4**, 611 (2010).
[19] D. N. Basov, M. M. Fogler, A. Lanzara, F. Wang, and Y. Zhang, Rev. Mod. Phys. **86**, 959 (2014).
[20] See Supplemental Material at http://link.aps.org/supplemental/10.1103/PhysRevB.93.161411 for relevant technical details.
[21] G. F. Giuliani and G. Vignale, *Quantum Theory of the Electron Liquid* (Cambridge University Press, Cambridge, U.K., 2005).
[22] A. Principi, M. Polini, and G. Vignale, Phys. Rev. B **80**, 075418 (2009).
[23] L. P. Kadanoff and G. Baym, *Quantum Statistical Mechanics* (W. A. Benjamin, New York, 1962).
[24] N. D. Mermin, Phys. Rev. B **1**, 2362 (1970).
[25] S. A. Mikhailov and K. Ziegler, Phys. Rev. Lett. **99**, 016803 (2007).
[26] I. Al-Naib, J. E. Sipe, and M. M. Dignam, Phys. Rev. B **90**, 245423 (2014).
[27] T. O. Wehling, A. Huber, A. I. Lichtenstein, and M. I. Katsnelson, Phys. Rev. B **91**, 041404(R) (2015).